Theoretical Study of Icosahedral *closo*-Borane, -Alane, and -Gallane Dianions ($A_{12}H_{12}^{2-}$; A = B, Al, Ga) with Endohedral Noble Gas Atoms (Ng = He, Ne, Ar, and Kr) and Their Lithium Salts ($Li[Ng@A_{12}H_{12}]^-$ and $Li_2[Ng@A_{12}H_{12}]$)

O. P. Charkin,*,†,‡,^ N. M. Klimenko†,§,^ D. Moran,^ A. M. Mebel,*,† D. O. Charkin,|| and P. v. R. Schleyer*,^

Institute of Atomic and Molecular Sciences, Academia Sinica, P.O. Box 23-166, Taipei 10764, Taiwan, Institute of Problems of Chemical Physics, Russian Academy of Sciences, Chernogolovka, Moscow Region, 142432 Russia, Lomonosov's Moscow State Academy of Fine Chemical Technology, Moscow, 117571 Russia, Center for Computational Quantum Chemistry, University of Georgia, Athens, Georgia 30602-2525, Department of Chemistry, Lomonosov's Moscow State University, Moscow, Russia

Received May 31, 2001

Geometries, energies, vibrational frequencies, and magnetic properties have been computed at the B3LYP level with the 6-31G* and 6-311+G* basis sets for a family of endohedral *closo*-boranes, -alanes, and -gallanes $Ng@A_{12}H_{12}^{2-}$ with noble gas atoms (Ng) located in the centers of icosahedral $[B_{12}]$, $[Al_{12}]$, and $[Ga_{12}]$ clusters. The endohedral structures of most of the systems are minima lying above separated Ng + $A_{12}H_{12}^{2-}$ by 166 ($He@B_{12}H_{12}^{2-}$) and 403 ($Ne@B_{12}H_{12}^{2-}$) kcal/mol for boranes; 29 ($He@Al_{12}H_{12}^{2-}$), 63 ($Ne@Al_{12}H_{12}^{2-}$), 154 ($Ar@Al_{12}H_{12}^{2-}$), and 189 ($Kr@Al_{12}H_{12}^{2-}$) kcal/mol for alanes; and 39 ($He@Ga_{12}H_{12}^{2-}$), 71 ($Ne@Ga_{12}H_{12}^{2-}$), and 213 ($Ar@Ga_{12}H_{12}^{2-}$) kcal/mol for gallanes. Three types of transition states are found for the exit of Ng from a cage: via an edge (**TS-1**), through a face (**TS-2**), and via a more extensive deformation through a pentagonal cage "neck" (**TS-3**). The most favorable exit path depends on the rigidity of the cage, the exothermicity of the dissociation, and the relationship between the size of the internal cavity of the cage and the Ng atomic radius. Ng exit via **TS-3** is preferred for $He@Al_{12}H_{12}^{2-}$, $Ne@Al_{12}H_{12}^{2-}$, $He@Ga_{12}H_{12}^{2-}$, $Ne@Ga_{12}H_{12}^{2-}$, $Ar@Al_{12}H_{12}^{2}$, and $Kr@Al_{12}H_{12}^{2-}$. Helium exits via a cage edge (**TS-1**) for $He@B_{12}H_{12}^{2-}$, while for $Ne@B_{12}H_{12}^{2-}$ the neon exits via a triangular face (**TS-2**). Exit barriers ($H_{exit}^{\ddagger}$) are high enough (30−60 kcal/mol) for all helium clusters and for $Ne@Al_{12}H_{12}^{2-}$ and $Ne@Ga_{12}H_{12}^{2-}$ to ensure the kinetic stability of these systems. The barriers for $Ar@Al_{12}H_{12}^{2-}$ and $Kr@Al_{12}H_{12}^{2-}$ decrease to 10−15 kcal/mol, while $Ne@B_{12}H_{12}^{2-}$ has a very low exit barrier and is not expected to be stable kinetically. There is a linear dependence of $Ng@A_{12}H_{12}^{2-}$ cage size on the Ng atomic radii; that is, the heavier Ng atoms "bulge" the cages. Nucleus independent chemical shifts (NICS) indicate that all three $A_{12}H_{12}^{2-}$ anions are aromatic but the alanes are the least so. A face- or edge-coordinated external Li^+ cation has a moderate effect on the structure and vibrational and magnetic properties of the helium-containing clusters, i.e., $Li[He@A_{12}H_{12}]^-$. In contrast, for systems with very large exothermicities of Ng exit, Li^+ complexation promotes their dissociation. Thus, the internal atom Ne exits from the cage of $Li[Ne@B_{12}H_{12}]^-$ and the salt dissociates into Ne + $LiB_{12}H_{12}^-$ without barrier. Systems with two Li^+ ions located initially above opposite cage faces ($Li_2[Ng@A_{12}H_{12}]$) undergo complex intramolecular rearrangements leading to destruction of the icosahedral closo structures.

Introduction

The preparation and characterization of polyhedral compounds containing endohedral atoms or ions ($X@A_n$) not only involve the fullerenes,[1] but also dodecahedrane $C_{20}H_{20}$[2] and metal clusters, such as Ga_{13}^-,[3] Tl_{13}^{11-}, $NiIn_{10}^{10-}$, $ZnIn_{10}^{10-}$, and $Ga_{19}[C(SiMe_3)_3]_6$[4a] and $Si@Al_{14}$.[4b] In addition, a number of more complex (condensed) clusters, which link small isolated molecular clusters and bulk metals,[2,5] also have been examined.[6]

Bombardment of cages such as fullerenes or dodecahedrane with ionized noble gas beams (Ng^+) followed by Ng NMR chemical shift measurement is a useful tool for the investigation of cluster structure and properties. In combination with ab initio calculations, this technique has been a fruitful approach to the study of isomerism, aromaticity, and other cluster properties.[7,8] Similarly, metals and alloys have been bombarded with Xe beams to form Xe_n clusters in the metal surface layers which

† Academia Sinica.
‡ Russian Academy of Sciences.
§ Lomonosov's Moscow State Academy of Fine Chemical Technology.
^ University of Georgia.
|| Lomonosov's Moscow State University.

(1) (a) Shabtai, E.; Weitz, A.; Haddon, R. C.; Hoffman, R. E.; Rabinovitz, M.; Khong, A.; Cross, R. J.; Saunders, M.; Cheng, P.-C.; Scott, L. T. *J. Am. Chem. Soc.* **1998**, *120*, 6389. (b) Shimshi, R.; Cross, R. J.; Saunders, M. J. *J. Am. Chem. Soc.* **1997**, *119*, 1163. (c) Cross, R. J.; Saunders, M.; Prinzbach, H. *Org. Lett.* **1999**, *1*, 1479. (d) Bühl, M.; Thiel, W.; Jiao, H.; Schleyer, P. v. R.; Saunders, M.; Anet, F. A. L. *J. Am. Chem. Soc.* **1994**, *116*, 6005. (e) Cioslowski, J. *Chem. Phys. Lett.* **1994**, *227*, 361. (f) Bühl, M.; Thiel, W. *Chem. Phys. Lett.* **1995**, *233*, 585. (g) Hirsch, A.; Chen, Z.; Jiao, H. *Angew. Chem., Int. Ed.* **2000**, *39*, 3915. (f) Rubin, Y.; Jarrosson, T.; Wang, G.-W.; Bartberger, M. D.; Houk, K. N.; Schick, G.; Saunders, M.; Cross, R. J. *Angew. Chem., Int. Ed.* **2001**, *40* , 1543. (g) Buhl, M. *Chem. Eur. J.* **1998**, *4*, 734.

(2) Jimenez-Vasquez, H. A.; Tamariz, J.; Cross, R. J. *J. Phys. Chem. A* **2001**, *105*, 1315.

(3) (a) Corbett, J. D. *Struct. Bond.* **1997**, *87*, 157. (b) Corbett, J. D. *Inorg. Chem.* **2000**, *39*, 5178. (c) Seo, D. K.; Corbett, J. D. *Science* **2001**, *291*, 841.

10.1021/ic010573s CCC: $20.00
Published on Web 11/30/2001

were then probed with Xe NMR spectroscopy to gain insight into the structure and properties of the metal surface layers and micrograin boundaries.[9]

Computational studies on endohedral polyhedral borane complexes include our[10a] examination of $He@B_{12}H_{12}^{2-}$ and $He@B_{17}H_{17}^{2-}$ and Jemmis and Balakrishnarajan's recent calculations on $B_{12}H_{12}^{2-}$ and $B_{14}H_{14}^{2-}$ dianions "stuffed" with cations C^{4+}, B^{3+}, Be^{2+}, Li^+, Al^{3+}, Mg^{2+}, and Zn^{2+},[11] as well as earlier studies on $B_6H_7^-$ and LiB_6H_7[10b] with proton and Li^+ in the center of the octahedral $B_6H_6^{2-}$ anion. Recently,[12] we reported preliminary results on a family of $X@Al_{12}H_{12}^{2-}$ alane and $X@Ga_{12}H_{12}^{2-}$ gallane endo clusters with inserted noble gas atoms He, Ne, Ar, and Kr, cations Li^+, Na^+, Be^{2+}, Mg^{2+}, Al^+, and Al^{3+}, and anions H^-, F^-, Cl^-, Br^-, O^{2-}, etc. However, these studies only characterized local minima for endo stuctures; the potential barriers for exit of heteroatoms from the cage were not calculated and the question of the kinetic stability of the endo isomers remained open. Among the issues of interest to chemists are the character of the interaction between the heteroatom and the cage, the peculiarities of the internal atom valence states, the influence of heteroatom on the cage, the limits of endohedral-cluster viability (i.e., which atoms inserted into a cage A_n result in kinetically stable species), the mechanism of intramolecular rearrangements between endo and exo isomers in salts, and the three-dimensional aromaticity of clusters with delocalized cage bonding such as fullerenes[1] and *closo*-boranes.[10a,13]

We now report the results of density functional (DFT) calculations on icosahedral *closo*-borane and model *closo*-alane and *closo*-gallane dianions ($A_{12}H_{12}^{2-}$; A = B, Al, or Ga) with noble gas atoms (Ng = He, Ne, Ar, and Kr) inserted in the center of the relatively small, dense cages ($Ng@A_{12}H_{12}^{2-}$). We also computed the lithium salts of several of these compounds, with one or two external Li cations ($Li[Ng@A_{12}H_{12}]^-$ and $Li_2[Ng@A_{12}H_{12}]$). Our investigation of the energetic and kinetic stabilities of the $Ng@A_{12}H_{12}^{2-}$ dianions reveals changes and trends in their structural and energetic parameters, vibrational frequencies, and NMR chemical shifts depending on the size of Ng and the cage, as well as the electronegativity of A. We analyze the influence of external cations on these properties and examine the differences between boranes, alanes, and gallanes. Our predictions on the structure, energetics, and spectroscopic properties of these compounds may be useful guides for the preparation and identification of new clusters. In contrast with the well-characterized dodecaborane dianion ($B_{12}H_{12}^{2-}$),[14] the corresponding parent alane ($Al_{12}H_{12}^{2-}$) and gallane ($Ga_{12}H_{12}^{2-}$) have not been reported to date. Nevertheless, we expect that our predictions should be applicable to recently synthesized icosahedral alane ($Al_{12}R_{12}^{2-}$)[15] and gallane ($Ga_{12}R_{10}^{2-}$)[16] anions which have bulky substituents (R = Bu, $N(SiH_3)_2$, $C_{13}H_9$, etc). Our earlier DFT calculations on fluoro-substituted boranes, $B_{12}H_iF_{12-i}$,[13a] and the substituted gallane series,[17] $Ga_{19}H_6^- - Ga_{19}(CH_3)_6^- - Ga_{19}[C(SiH_3)_3]_6^-$, revealed that the skeleton geometry is relatively insensitive to the external substituent.

Computational Methods

Similar to our previous computational studies,[12] all geometries (see Figure 1) were optimized using the hybrid density functional B3LYP method[18] with the standard 6-31G* basis set; vibrational frequencies were computed at the same B3LYP/6-31G* level of theory. The borane anions were then reoptimized with the more flexible 6-311+G** basis set while the alanes and all salts were refined by computing B3LYP/6-311+G** single points, i.e., B3LYP/6-311+G**//B3LYP/6-31G*. Gallanes were only computed at B3LYP/6-31G*. Optimized $B_{12}H_{12}^{2-}$ and $Al_{12}H_{12}^{2-}$ R(A−A) anion bond lengths (Table 1) reproduce X-ray R(B−B) and R(Al−Al) values[14,15] satisfactorily. B3LYP/6-31G*

(4) (a) Schnepf, A.; Stösser, G.; Schnökel, H. *J. Am. Chem. Soc.* **2000**, *122*, 9178. (b) Purath, A.; Dohmeier, A.; Ecker, A.; Schnökel, H.; Ahlrichs, R.; Stoermer, C.; Friedrich, J.; Jutzi, P. *J. Am. Chem. Soc.* **2000**, *122*, 6955.

(5) Dohmeier, C.; Loos, D.; Schnökel, H. *Angew. Chem., Int. Ed. Engl.* **1996**, *35*, 129.

(6) (a) Schnepf, A.; Weckert, E.; Linti, G.; Schnökel, H. *Angew. Chem., Int. Ed.* **1999**, *38*, 3381. (b) Linti, G.; Rodig, A. *Chem. Commun.* **2000**, 127. (c) Schnepf, A.; Schnökel, H. *Angew. Chem., Int. Ed.* **2001**, *40*, 712.

(7) (a) Shabtai, E.; Weitz, A.; Haddon, R. C.; Hoffman, R. E.; Rabinovitz, M.; Khong, A.; Cross, R. J.; Saunders, M.; Cheng, P.-C.; Scott, L. T. *J. Am. Chem. Soc.* **1998**, *120*, 6389. (b) Shimshi, R.; Cross, R. J.; Saunders, M. J. *J. Am. Chem. Soc.* **1997**, *119*, 1163. (c) Bühl, M.; Thiel, W.; Jiao, H.; Schleyer, P. v. R.; Saunders, M.; Anet, F. A. L. *J. Am. Chem. Soc.* **1994**, *116*, 6005. (d) Cioslowski, J. *Chem. Phys. Lett.* **1994**, *227*, 361. (e) Bühl, M.; Thiel, W. *Chem. Phys. Lett.* **1995**, *233*, 585. (f) Hirsch, A.; Chen, Z.; Jiao, H. *Angew. Chem., Int. Ed.* **2000**, *39*, 3915. (g) Rubin, Y.; Jarrosson, T.; Wang, G.-W.; Bartberger, M. D.; Houk, K. N.; Schick, G.; Saunders, M.; Cross, R. J. *Angew. Chem., Int. Ed.* **2001**, *40*, 1543. (h) Buhl, M. *Chem. Eur. J.* **1998**, *4*, 734.

(8) (a) Cross, R. J.; Saunders, M.; Prinzbach, H. *Org. Lett.* **1999**, *1*, 1479. (b) Jimenez-Vasquez, H. A.; Tamariz, J.; Cross, R. J. *J. Phys. Chem. A* **2001**, *105*, 1315.

(9) (a) Allen, C. W.; Song, M. H.; Furuya, K.; et al. *J. Electron Microsc.* **1999**, *48*, 503. (b) Birtcher, R. C.; Furuya, K.; Allen, C. W.; Song, M.; Mitsuishi, K.; Donnelly, S. E. *Nucl. Instrum. Methods B* **1999**, *148*, 184.

(10) (a) Schleyer, P. v. R.; Narafian, K.; Mebel, A. M. *Inorg. Chem.* **1998**, *37*, 6765. (b) Mebel, A. M.; Charkin, O. P.; Kuznetsov, I. Yu.; Solntsev, K. A.; Kuznetsov, N. T. *Russ. J. Inorg. Chem. (Engl. Transl.)* **1988**, *33*, 958.

(11) Jemmis, E. D.; Balakrishnarajan, M. M. *J. Am. Chem. Soc.* **2000**, *122*, 7392.

(12) (a) Charkin, O. P.; Klimenko, N. M.; Schleyer. P. v. R. *Russ. J. Inorg. Chem. (Engl. Transl.)* **2000**, *45*, 1539. (b) Charkin, O. P.; Klimenko, N. M.; Moran, D.; Mebel, A. M.; Schleyer. P. v. R. *Russ. J. Inorg. Chem. (Engl. Transl.)* **2001**, *46*, 110.

(13) (a) Solntsev, K. A.; Mebel, A. M.; Votinova, N. A.; Kuznetsov, N. T.; Charkin, O. P. *Koord. Khim.* **1992**, *18*, 340. (b) Schleyer, P. v. R.; Jiao, H. *Pure Appl. Chem.* **1996**, *68*, 209.

(14) (a) Lipscomb, W. N. *Boron Hydrides*; W. A. Benjamin: New York, 1963. (b) Muetterties, E. L. *Boron Hydride Chemistry*; Academic Press: New York, 1975. (c) Olah, G. A.; Surya Prakash, G. K.; Williams, R. E.; Field, L. D.; Wade, K. *Hypercarbon Chemistry*; Wiley: New York, 1987. (d) Liebman, J. F.; Greenberg, A.; Williams, R. E. *Advances in Boron and the Boranes*; VCH Verlagsgesellschaft: New York, 1988. (e) Wade, K. *Electron Deficient Compounds*; Nelson: London, 1971. (f) Minkin, V. I.; Minyaev, R. M.; Zhdanov, Yu. A. *Nonclassical Structures of Organic Compounds*; Mir Publishers: Moscow, 1987. (g) Mingos, D. M. P.; Wales, D. J. *Introduction to Cluster Chemistry*; Prentice Hall: Englewood Cliffs, NJ, 1990. (h) Olah, G. A.; Wade, K.; Williams, R. E. *Electron Deficient Boron and Carbon Clusters*; John Wiley and Sons: New York, 1991. (i) Williams, R. E. *Chem. Rev.* **1992**, *92*, 177. (j) Williams, R. E. In *Advances in Organometallic Chemistry*; Stone, F. G. A., West, R., Eds.; Academic Press: New York, 1994. (k) Schleyer, P. v. R.; Subramanian, G.; Dransfeld, A. *J. Am. Chem. Soc.* **1996**, *118*, 9988. (l) Schleyer, P. v. R.; Subramanian, G.; Jiao, H.; Najafian, K.; Hofmann, M. In *Advances in Boron Chemistry*; Siebert, W., Ed.; The Royal Society of Chemistry: Cambridge, England, 1997. (m) Schleyer, P. v. R.; Najafian, K. In *The Borane, Carborane, Carbocation Continuum*; Casanova, J., Ed.; Wiley: New York, 1998. (n) Schleyer, P. v. R.; Najafian, K. *Inorg. Chem.* **1998**, *37*, 3454. (o) Brown, L. D.; Lipscomb, W. N. *Inorg. Chem.* **1977**, *16*, 2989. (p) Bicerano, J.; Marynick, D. S.; Lipscomb, W. N. *Inorg. Chem.* **1978**, *17*, 3443. (q) Bicerano, J.; Marynick, D. S.; Lipscomb, W. N. *Inorg. Chem.* **1978**, *17*, 2041.

(15) Hiller, W.; Klinkhammer, K.-W.; Uhl, W.; Wagner, J. *Angew. Chem.* **1991**, *B. 103*, 182.

(16) Schnepf, A.; Stösser, G.; Köppe, R.; Schnökel, H. *Angew. Chem., Int. Ed.* **2000**, *39*, 1637.

(17) Charkin, O. P.; Klimenko, N. M.; Schleyer, P. v. R. Unpublished results.

(18) (a) Becke, A. D. *J. Chem. Phys.* **1993**, *98*, 5648. (b) Lee, C.; Yang, W.; Parr, R. G. *Phys. Rev. B* **1988**, *B37*, 785.

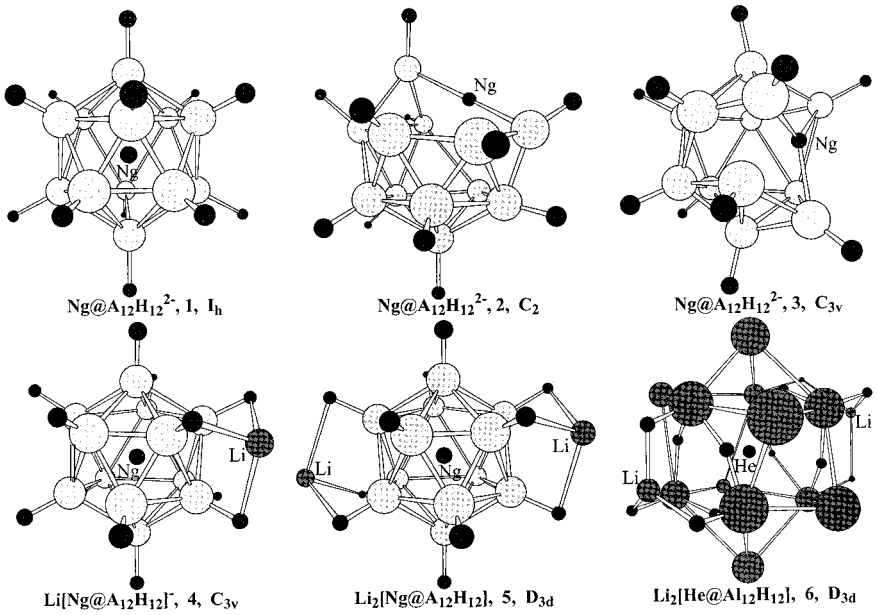

Figure 1. Various $Ng@A_{12}H_{12}^{2-}$, $Li[Ng@A_{12}H_{12}]^-$, and $Li_2[Ng@A_{12}H_{12}]$ geometries.

Table 1. Calculated[a] Bond Lengths (Å) of *closo*-Boranes, -Alanes, and -Gallanes $Ng@A_{12}H_{12}^{2-}$[b] (**1**,I_h) with Ng Atoms[c] in the Center of the $[A_{12}]$ Icosahedron

	B			Al					Ga			
	empty[d]	He	Ne	empty[d]	He	Ne	Ar	Kr	empty[d]	He	Ne	Ar
R(Ng−A)	(1.700)	1.770	1.904	(2.569)	2.597	2.635	2.724	2.758	(2.453)	2.487	2.546	2.635
R(A−A)	1.787	1.861	2.002	2.703	2.730	2.770	2.864	2.900	2.579	2.614	2.677	2.823
R(A−H)	1.202	1.202	1.202	1.605	1.609	1.610	1.613	1.616	1.568	1.569	1.571	1.584

[a] At B3LYP/6-311+G** for boranes and B3LYP/6-31G* for alanes and gallanes. The basis set extension from 6-31G* to 6-311+G* does not effect the borane results significantly. [b] A = B, Al, Ga. [c] Ng = "empty", He, Ne, Ar, Kr. [d] Values for isolated $A_{12}H_{12}^{2-}$ dianions calculated at the same levels of theory. In parentheses, the distance from the icosahedron center to a vertex atom, A.

magnetic shielding constants and NMR chemical shifts were computed with the GIAO method.[19] All calculations employed the Gaussian 98 program package.[20] Results are presented in Tables 1−5, and optimized structures are shown in Figures 1 and 3.

Results and Discussion

Geometric and Energetic Parameters. Local minima exist for most but not all endohedral icosahedral anions $Ng@A_{12}H_{12}^{2-}$. I_h minima include $He@B_{12}H_{12}^{2-}$ and $Ne@B_{12}H_{12}^{2-}$ as well as the entire alane series (He−Kr). The $Ng@Ga_{12}H_{12}^{2-}$ I_h configuration stability only includes He, Ne, and Ar.[21] The remaining $Ng@A_{12}H_{12}^{2-}$ structures have one or several degenerate imaginary frequencies; these endohedral icosahedral structures are not stable with respect to exit of the inserted atom from the cage.

As expected,[12] all endohedral icosahedral clusters are higher in energy than the empty cage plus the Ng atom. E_{diss}, the zero-point vibrational energy (ZPE) corrected energies released during dissociation

$$Ng@A_{12}H_{12}^{2-} \rightarrow Ng + A_{12}H_{12}^{2-}$$

are (see Table 2) 166 ($He@B_{12}H_{12}^{2-}$) and 403 ($Ne@B_{12}H_{12}^{2-}$) kcal/mol for boranes, 29 ($He@Al_{12}H_{12}^{2-}$), 63 ($Ne@Al_{12}H_{12}^{2-}$), 154 ($Ar@Al_{12}H_{12}^{2-}$), and 189 ($Kr@Al_{12}H_{12}^{2-}$) kcal/mol for alanes, 39 ($He@Ga_{12}H_{12}^{2-}$), 71 ($Ne@Ga_{12}H_{12}^{2-}$), and 213 ($Ar@Ga_{12}H_{12}^{2-}$) kcal/mol for gallanes. While E_{diss} increases with larger noble gas atomic radii R(Ng), the trend with cage size is irregular (boranes > alanes < gallanes). This trend is in line with the cage sizes as gallanes are more compact than the alanes; the lengths of the R(Ga−Ga) edges as well as the peripheral R(Ga−H) bonds are shorter than the corresponding R(Al−Al) and R(Al−H) distances by 0.12 and 0.04 Å, respectively, both in the empty $A_{12}H_{12}^{2-}$ dianions and in the endohedral $Ng@A_{12}H_{12}^{2-}$ systems (Table 1). In turn, the larger size of alanes as compared to gallanes may be related to the order of electronegativities, B > Al < Ga. Al is less electronegative than Ga and forms more ionic bonds with H's, thus making the Al_{12} cage more electron deficient and weakly bound than Ga_{12}.

The sizes of the endohedral clusters increase upon Ng encapsulation, parallel with the rise in their dissociation exothermicity. Compared with the B−B length in the empty dianion,

(19) (a) Ditchfield, R. *Mol. Phys.* **1974**, *27*, 789. (b) Wolinski, K.; Hilton, J. F.; Pulay, P. *J. Am. Chem. Soc.* **1990**, *112*, 8251.

(20) Frisch, M. J.; Trucks, G. W.; Schlegel, H. B.; Scuseria, G. E.; Robb, M. A.; Cheeseman, J. R.; Zakrzewski, V. G.; Montgomery, J. A., Jr.; Stratmann, R. E.; Burant, J. C.; Dapprich, S.; Millam, J. M.; Daniels, A. D.; Kudin, K. N.; Strain, M. C.; Farkas, O.; Tomasi, J.; Barone, V.; Cossi, M.; Cammi, R.; Mennucci, B.; Pomelli, C.; Adamo, C.; Clifford, S.; Ochterski, J.; Petersson, G. A.; Ayala, P. Y.; Cui, Q.; Morokuma, K.; Malick, D. K.; Rabuck, A. D.; Raghavachari, K.; Foresman, J. B.; Cioslowski, J.; Ortiz, J. V.; Baboul, A. G.; Stefanov, B. B.; Liu, G.; Liashenko, A.; Piskorz, P.; Komaromi, I.; Gomperts, R.; Martin, R. L.; Fox, D. J.; Keith, T.; Al-Laham, M. A.; Peng, C. Y.; Nanayakkara, A.; Gonzalez, C.; Challacombe, M.; Gill, P. M. W.; Johnson, B.; Chen, W.; Wong, M. W.; Andres, J. L.; Head-Gordon, M.; Replogle, E. S.; Pople, J. A. *Gaussian 98*, Revision A.7; Gaussian, Inc.: Pittsburgh, PA, 1998.

(21) All $Ar@Ga_{12}H_{12}^{2-}$ vibrational frequencies are real at the Hartree−Fock level; however, B3LYP gives one small imaginary frequency of 22i cm^{-1}. The character of this icosahedral stationary point needs to be determined by higher level calculations.

Table 2. Total Energies (au), ZPE, Dissociation Energies of $Ng@A_{12}H_{12}^{2-}$, Deformation Energies of the Cage $A_{12}H_{12}^{2-}$ due to Insertion of Ng, Relative Energies of Structures **2** and **3**, and Barriers for Exit of Ng from the Cage $A_{12}H_{12}^{2-}$ in *closo*-Boranes, -Alanes, and -Gallanes (kcal/mol)[a]

	$Ng@Al_{12}H_{12}^{2-}$			
Ng	He	Ne	Ar	Kr
E_{tot}	−2919.8036	−3045.7949	−3444.2410	−5670.3744
ZPE	60.2	59.2	57.8	56.9
E_{diss}[b]	−29.1	−62.9	−154.3	−188.8
E_{def}	0.9	5.3	26.0	37.3
$E_{rel}(\mathbf{2},C_2)$[c]	78.8	39.3	−36.0	−59.2
$E_{rel}(\mathbf{3},C_{3v})$[c]	77.2	48.7	−0.4	−21.7
$H_{exit}^{\ddagger}$	58.5	41.5	15.2	10.5

	$Ng@B_{12}H_{12}^{2-}$		$Ng@Ga_{12}H_{12}^{2-}$[d]	
Ng	He	Ne	He	Ne
E_{tot}	−308.4141	−434.0679	−23058.8081	−23122.7381
ZPE	106.8	97.2	57.6	55.9
E_{diss}[b]	−166.0	−402.9	−38.7	−70.9
E_{def}	15.4	104.1	1.5	11.8
$E_{rel}(\mathbf{2},C_2)$[c]	31.2	−170.0		
$E_{rel}(\mathbf{3},C_{3v})$[c]	97.1	−88.8		
$H_{exit}^{\ddagger}$	63.5	2.6	29.1[e]	

[a] Calculations of E_{tot} and E_{diss} were performed at the B3LYP/6-311+G** level for boranes, B3LYP/6-311+G**//B3LYP/6-31G* for alanes, and B3LYP/6-31G* for gallanes, while the other energies (ZPE, E_{def}, E_{rel}, and $H_{exit}^{\ddagger}$) were calculated at the B3LYP/6-31G* level. E_{tot} and ZPE for empty clusters are the following: −305.7638, −2919.9334, and −23082.9584 au and 105.0, 58.0, and 54.9 kcal/mol for $B_{12}H_{12}^{2-}$, $Al_{12}H_{12}^{2-}$, and $Ga_{12}H_{12}^{2-}$, respectively. [b] The dissociation limit corresponds to dissociation of $Ng@A_{12}H_{12}^{2-}$ (**1**) into $Ng + A_{12}H_{12}^{2-}$. [c] With respect to the energy of the icosahedral $Ng@A_{12}H_{12}^{2-}$ structure **1**. [d] For $Ar@Ga_{12}H_{12}^{2-}$ E_{tot}, ZPE, and E_{diss} are the following: −23610.1339 au, 58.3, and −217.8 kcal/mol, respectively. [e] Calculated at the B3LYP/SDD level.

the B−B edge in the boranes elongates by 0.08 and 0.21 Å after insertion of He and Ne, respectively. In the alanes, where the empty cage size is larger, the Al−Al edge elongations when He and Ne are inserted are only 0.03 and 0.07 Å, respectively, but this increases to 0.16 and 0.20 Å, respectively, upon insertion of Ar and Kr. The cage expansion in gallanes is similar to that in alanes. The peripheral $Ng@A_{12}H_{12}^{2-}$ A−H bonds are also stretched but only by a few thousandths of an angstrom.

As shown in Figure 2a, the changes in $Ng@A_{12}H_{12}^{2-}$ edge ΔR(A−A) and radial ΔR(Ng−A) distances exhibit nearly linear dependences on the noble gas atomic radius R(Ng)

$$\Delta R(\mathrm{Ng-A}) \sim K_A R(\mathrm{Ng})$$

where the coefficient K_A is largest for boranes, smallest for alanes, and is intermediate for gallanes. Dissociation energies calculated for clusters with internal He, Ne and Ar atoms show a parabolic dependence on ΔR(Ng−A) with a minor quadratic term (Figure 2b).

To estimate cage deformation energies due to Ng insertion, $E_{def}(A_{12}H_{12}^{2-})$, we carried out single-point B3LYP/6-31G* calculations on the expanded empty $A_{12}H_{12}^{2-}$ dianion geometries based on the equilibrium structures of endohedral $Ng@A_{12}H_{12}^{2-}$ clusters. These were compared with the energies of the fully relaxed $A_{12}H_{12}^{2-}$ dianions (energies given in Table 2). As expected from the results discussed above, the alane cage appears to be more "elastic" with respect to expansion than the borane cage while the gallane cage is intermediate. In the rigid borane clusters, even replacement of He with Ne leads to elongation of R(B−B) by 0.13 Å and sharp increases in E_{diss} (∼237 kcal/mol) and in E_{def} (∼90 kcal/mol). In contrast, replacement of He with a much larger analogue, Kr, in the "elastic" alane cage elongates R(Al−Al) to a similar extent (0.16 Å), but the E_{diss} and E_{def} energies increase by only ∼150 and ∼36 kcal/mol, respectively. Apparently, the higher rigidity of the $Ga_{12}H_{12}^{2-}$ dianion is responsible for the instability of the icosahedral $Kr@Ga_{12}H_{12}^{2-}$ cluster. The dependence of the change of empty cluster total energy $[\Delta E_{tot}(A_{12}H_{12}^{2-})]$ for the boranes and alanes families on the change in their size ΔR(oA) (o is the center of the icosahedron) is described by two parabolic curves, shown in Figure 2c, the flat one for the "elastic" alanes and the steeper one for the more rigid boranes. The good fit, together with the linear dependence of $Ng@A_{12}H_{12}^{2-}$ cluster size on R(Ng), indicates that steric repulsion is the dominant factor determining the compactness and strain energy of a cage. Since the steepest rise in R(Ng) occurs between Ne and Ar, the largest change in endohedral alane structural and energetic parameters also takes place when Ne is replaced with Ar. However, replacements of He by Ne and Ar by Kr result in smaller changes.

Clearly, cage deformation energy constitutes only a small fraction of the energy released when an internal Ng atom is expelled from a cage. E_{def} is small for $He@Al_{12}H_{12}^{2-}$ and $He@Ga_{12}H_{12}^{2-}$, moderate for their Ne analogues (5−10 kcal/mol), and becomes significant only with Ng = Ar. Rigid boranes again behave differently; for $He@B_{12}H_{12}^{2-}$ E_{def} is 15 kcal/mol and increases to 104 kcal/mol for $Ne@B_{12}H_{12}^{2-}$. Obviously, strong repulsive interactions between the noble gas atom and the cage contribute strongly to E_{diss}.

Vibrational Frequencies. Vibrational frequencies involving $Ng@A_{12}H_{12}^{2-}$ cage atoms and peripheral bonds may be shifted (either blue or red) compared with the corresponding frequencies of the empty $A_{12}H_{12}^{2-}$ anions (Table 3). The frequencies usually shift monotonically with increase in Ng atomic number. For example, the lowest $1h_g$, $1g_g$, and $2h_g$ frequencies in the alane series decrease by 50−60 cm^{-1} in going from He to Kr; the larger Al−H stretching frequencies ($4h_g$, $2t_{2u}$, $2a_{1g}$, and $4t_{1u}$) decrease uniformly by ∼40 cm^{-1}, and the $3h_g$ frequencies increase by 40 cm^{-1}. Only four t_{1u} frequencies are IR active due to the high I_h symmetry. Among these, the changes of most intense vibrations ($3t_{1u}$ and $4t_{1u}$) are small and the vibration with the largest frequency shift ($1t_{1u}$) has a low intensity. Therefore, the $2t_{1u}$ vibration, in the 925−1030 cm^{-1} range for boranes and 340−560 cm^{-1} for alanes and gallanes, which for the most part corresponds to motions of the inserted Ng atom and of moderate intensity, should be the most informative in IR spectroscopic studies of the endohedral clusters.

Orbital Energies, Population Analysis, and Charge Distribution. Endohedral alanes and gallane ionization potentials (IP), evaluated using Koopmans' theorem (Table 4), show only a weak dependence on Ng and are close to those of the empty $Al_{12}H_{12}^{2-}$ and $Ga_{12}H_{12}^{2-}$ dianion IPs (1.0−1.1 eV). In contrast, the $Ng@B_{12}H_{12}^{2-}$ IPs decrease significantly from the empty $B_{12}H_{12}^{2-}$ (∼1.6 eV) to $Ne@B_{12}H_{12}^{2-}$ (∼1.1 eV). The HOMO−LUMO separations decrease with increasing Ng radius and range from 8 to 9.5 eV in alanes and gallanes and 10−11.5 eV in boranes. The skeleton valence molecular orbitals (MO) energy levels and those of the atomic orbitals (AO) of the internal He and Ne atoms are well separated and do not mix. The Ar and Kr AO and the skeleton valence MO levels do approach each other. Hence, the cage bonding t_{1u} MO includes some contribution from a p AO of these noble gas atoms. For example, the Ar 3p AO and Kr 4p AO population in the alane cage t_{1u} MOs are ∼0.3 and ∼0.4 *e*, respectively. The situation is similar for the $Ng@B_{12}H_{12}^{2-}$ clusters (the contribution of the $1s_{He}$ and $2p_{Ne}$

Table 3. Calculated[a] Vibrational Frequencies ν_i (cm^{-1}) of *closo*-Boranes, -Alanes, and -Gallanes $Ng@A_{12}H_{12}^{2-}$ [b] (**1**,I_h) with Ng Atoms[c] in the Center of the [A_{12}] Icosahedron

		B			Al					Ga		
		empty[d]	He	Ne	empty[d]	He	Ne	Ar	Kr	empty[d]	He	Ne
h_u	1	521	439	291	174	163	149	115	103	92	80	60
	2	959	932	879	486	491	489	481	473	488	497	492
h_g	1	575	573	369	185	204	204	192	183	114	128	122
	2	765	713	687	328	316	302	274	269	219	209	196
	3	962	912	888	466	472	486	504	513	450	464	482
	4	2517	2526	2526	1804	1810	1805	1790	1775	1883	1880	1861
g_u	1	747	612	328	307	294	271	219	204	200	188	163
	2	879	883	834	426	471	468	488	487	426	475	477
g_g	1	662	569	404	246	233	218	181	170	148	136	117
	2	946	898	867	450	450	458	458	456	433	441	448
t_{1u}	1	710	574	294	309	283	233	190	158	212	193	161
		(7)	(1)	(0)	(5)	(3)	(1)	(1)	(1)	(0)	(0)	(0)
	2		1031	925		456	357	376	338		585	376
			(77)	(71)		(10)	(6)	(10)	(10)		(12)	(3)
	3	1089	1343	1003	578	580	579	565	550	567	562	569
		(64)	(15)	(53)	(288)	(287)	(303)	(294)	(264)	(218)	(227)	(254)
	4	2535	2544	2542	1810	1816	1812	1798	1784	1883	1880	1863
		(1149)	(1225)	(1359)	(1656)	(1700)	(1742)	(1884)	(1964)	(1656)	(1679)	(1719)
t_{2u}	1	765	743	747	253	255	266	267	270	155	156	167
	2	2510	2519	2520	1800	1806	1802	1788	1774	1876	1872	1857
t_{1g}	1	961	941	899	420	425	422	414	407	387	389	373
a_g	1	744	704	659	299	297	297	273	274	208	204	198
	2	2572	2583	2580	1834	1841	1836	1823	1811	1910	1907	1890

[a] At the B3LYP/6-31G* level. Intensities of IR-active t_{1u} vibrations (km/mol) are given in parentheses. The $Ar@B_{12}H_{12}^{2-}$ and $Ng@Ga_{12}H_{12}^{2-}$ clusters with Ng = Ar and Kr possess one or several degenerate imaginary frequencies. [b] A = B, Al, Ga. [c] Ng = "empty", He, Ne, Ar, Kr. [d] Data for the isolated $A_{12}H_{12}^{2-}$ species at the same level of theory.

Table 4. Orbital Energies (au) of $A_{12}H_{12}^{2-}$ MOs and Effective Atomic Charges (*e*) of $A_{12}H_{12}^{2-}$ and $Ng@A_{12}H_{12}^{2-}$ [b] Calculated at the HF/6-31G*//B3LYP/6-31G* Level

	B			Al				
	empty[a]	He	Ne	empty[a]	He	Ne	Ar	Kr
MO								
a_g		−0.956	−1.819		−0.825	−1.835	−1.204	−1.071
t_{1u}			−0.791			−0.761	−0.565	−0.526
a_g	−0.706	−0.493	−0.563	−0.466	−0.433	−0.446	−0.419	−0.405
t_{1u}	−0.523	−0.517	−0.421	−0.382	−0.382	−0.367	−0.332	−0.313
h_g	−0.327	−0.325	−0.327	−0.287	−0.288	−0.289	−0.293	−0.295
t_{2u}	−0.217	−0.230	−0.253	−0.254	−0.256	−0.258	−0264.	−0.266
a_g	−0.301	−0.184	−0.236	−0.232	−0.213	−0.221	−0.210	−0.201
t_{1u}	−0.202	−0.212	−0.145	−0.193	−0.197	−0.185	−0.156	−0.131
h_g	−0.105	−0.111	−0.120	−0.123	−0.125	−0.127	−0.138	−0.144
g_u	−0.056	−0.049	−0.038	−0.037	−0.037	−0.037	−0.038	−0.038
g* LUMO	0.501	0.482	0.441	0.276	0.274	0.270	0.262	0.259
Z								
Ng		0.07	0.04		0.02	0.06	0.32	0.31
A	−0.05	−0.05	−0.02	−0.00	−0.00	−0.00	−0.02	−0.02
H	−0.12	−0.12	−0.15	−0.16	−0.17	−0.17	−0.17	−0.18

[a] Data for the isolated $A_{12}H_{12}^{2-}$ species at the same level of theory. [b] A = B, Al. Ng = "empty", He, Ne, Ar, Kr.

AO into the a_g and t_{1u} MO are 0.3 and 0.2 *e*, respectively) since the $B_{12}H_{12}^{2-}$ dianion valence orbital levels lie much lower than those in $Al_{12}H_{12}^{2-}$. The a_g and t_{1u} MOs show the strongest dependence of orbital energetic levels on the nature of the internal Ng atoms.

Both Mulliken and natural bond orbital (NBO) population analyses on the alanes and gallanes show nearly zero charges on He and Ne. Only a small charge transfer from their heavier analogues (which increases slightly from Ar to Kr but does not exceed 0.1 *e*) occurs to the $A_{12}H_{12}$ cage. A similarly small charge transfer takes place in boranes where the He and Ne charges are +0.05 and +0.10 *e*. The overlap populations *Q*(Ng−A) are negative and decrease in alanes from $He@Al_{12}H_{12}^{2-}$ (−0.02 *e*) to $Kr@Al_{12}H_{12}^{2-}$ (−0.15 *e*). Positive *Q*(A−A) overlap populations decrease slowly when the cage strain increases, while *Q*(A−H) populations for the peripheral bonds are rather insensitive to the nature of Ng. These results once more indicate that steric repulsion between Ng and cage is the dominant force in endohedral clusters with noble gases.

Magnetic Shielding Constants and NMR Chemical Shifts. Depending on the size, shape, and charge of the cluster, ^{3}He chemical shifts inside fullerene cages are −8 to −48 ppm compared to free He.[1] The negative sign of the ^{3}He NMR chemical shift δ(He) is due to the shielding effect induced by the cyclic electron delocalization in the π-electronic system (i.e., aromaticity) of the C_n cluster. In the icosahedral $Ng@A_{12}H_{12}^{2-}$ clusters, the internal Ng and cage atoms are closer together than in the larger endo-fullerenes. *closo*-Boranes are known to exhibit

Table 5. Magnetic Shielding Constants σ and Nucleus Independent Chemical Shifts (NICS) of $A_{12}H_{12}^{2-}$ Closo Anions (A = B, Al, and Ga) and $Ng@A_{12}H_{12}^{2-}$ Endo Clusters (ppm)[a]

	σ			NICS[b]			
anion	A	Ng	H	(c)	(0)	(0.5)	(1.0)
$B_{12}H_{12}^{2-}$	127.0		30.8	25.9	−48.4	−30.7	−9.5
$He@B_{12}H_{12}^{2-}$	122.4	82.0	30.8		−47.0	−33.6	−9.4
$Ne@B_{12}H_{12}^{2-}$	110.1	38.1	29.7		−40.2	−25.7	−8.0
$Al_{12}H_{12}^{2-}$	575.2		29.8	−20.5	−28.1	−21.9	−11.8
$He@Al_{12}H_{12}^{2-}$	572.9	78.2	29.8		−27.6	−20.7	−10.7
$Ne@Al_{12}H_{12}^{2-}$	575.6	400.2	29.7		−26.5	−19.9	−10.3
$Ar@Al_{12}H_{12}^{2-}$	588.2	752.5	29.5		−23.7	−18.1	−9.3
$Kr@Al_{12}H_{12}^{2-}$	602.9	2259.3	29.3		−21.6	−16.9	−8.7
$Ga_{12}H_{12}^{2-}$	2191.0		30.0	−25.5	−36.3	−26.8	−13.0
$He@Ga_{12}H_{12}^{2-}$	2199.7	82.9	30.0		−35.4	−26.0	−12.7
$Ne@Ga_{12}H_{12}^{2-}$	2236.1	332.0	29.8		−32.9	−24.4	−12.0
$Ar@Ga_{12}H_{12}^{2-}$	2313.0	581.4	29.2		−27.1	−20.7	−10.3

[a] Calculated at the GIAO/B3LYP/6-31G* level. Absolute shieldings (σ) are presented. Calculations at the same level of theory give the following magnetic shielding constants (in ppm) for AlH_4^- (σ(Al) = 541), GaH_4^- (σ(Ga) = 2008), and B_2H_6 (σ(B) = 28.1), for which the accepted experimental NMR chemical shifts are δ(Al) = 100−103, δ(Ga) = 682, and δ(B) = 16.6 ppm. Ng isotropic shielding constants are 59.8, 552.0, 1237.0, and 3236.0 ppm for He, Ne, Ar, and Kr, respectively. [b] The NICS values were calculated at the centers of the icosahedron (c) and of a face (0) as well as at the 0.5 and 1.0 Å distances above a face center ((0.5) and (1.0), respectively).

three-dimensional aromaticity due to the multicenter skeletal bonding.[10a,13] The computed NMR chemical shifts, δ(He), for $He@A_{12}H_{12}^{2-}$ clusters depend on the size and nature of the $A_{12}H_{12}^{2-}$ cage. Nucleus independent chemical shifts (NICS)[22] were also computed as an aromaticity criteria and are included in Table 5. NICS were calculated in the centers of the cages, and of the faces, as well as 0.5 and 1.0 Å above the face centers of both the empty $A_{12}H_{12}^{2-}$ dianions and $He@A_{12}H_{12}^{2-}$ clusters.

Akin to the fullerenes, $He@A_{12}H_{12}^{2-}$ icosahedron He chemical shifts (δ(He)) are negative with respect to free He (i.e., shielding in all three cages) but are 2−2.5 times larger compared with δ(He) for $He@C_{60}$. Interestingly, δ(He) does not vary regularly along the $A_{12}H_{12}^{2-}$ (A = B−Al−Ga) series; the δ(He) values are similar (−22.2 and −23.1 ppm) in the borane and gallane complexes but only −18.4 ppm in the alane. A comparable trend is observed for NICS values in the center of the free $A_{12}H_{12}^{2-}$ dianions (−25.9 and −25.5 ppm for $B_{12}H_{12}^{2-}$ and $Ga_{12}H_{12}^{2-}$, respectively, vs −20.5 ppm for $Al_{12}H_{12}^{2-}$). Note that other properties of the closo systems (documented above) exhibited similar irregular changes down group 13. The alanes have the largest cages and are the most flexible with respect to deformations. The magnetic criteria indicate that alane clusters are less aromatic than both the boranes and the gallanes.

In spacious fullerene cages like C_{60} the chemical shifts of endohedral He and Ne atoms are nearly identical.[1e] In contrast, in dense cages like $Ne@B_{12}H_{12}^{2-}$, $Ar@Al_{12}H_{12}^{2-}$, and $Kr@Al_{12}H_{12}^{2-}$, where the internal pressure is high and cage deformation approaches the threshold, the δ(Ne), δ(Ar), and δ(Kr) chemical shifts change sign from negative to positive and increase sharply (+513.9, +484.5, and +976.7 ppm, respectively). In principle, one can think that the use of heavier rare gas atoms to probe dense endo clusters would be more informative than the use of light Ng's. For instance, our calculations indicate that in alanes and gallanes the changes of δ(He) from the $He@A_{12}H_{12}^{2-}$ anion to $Li^+[He@A_{12}H_{12}^{2-}]$ with a face-coordinated external cation Li^+ do not exceed few parts per million, while in their Ne analogues the changes are several times larger.

Transition States and Potential Barriers for Endohedral Clusters. Since all $Ng@A_{12}H_{12}^{2-}$ clusters considered here are higher in energy than dissociated Ng + $A_{12}H_{12}^{2-}$, the barrier heights ($H_{exit}^{\ddagger}$) for Ng expulsion from the cage provide information about their kinetic stability. Our preliminary estimates of $H_{exit}^{\ddagger}$ provided general indications of stability but only employed partially optimized (B3LYP/6-31G*) "surface" structures **2**, C_2, and **3**, C_{3v}, where the Ng's were positioned at the center of an edge or of a face, respectively.[12] The search for the real transition states (TS) is far more demanding due to the complexity of the opening of the $Ng@A_{12}H_{12}^{2-}$ cages and the motions of the exiting heteroatom. For instance, for the $He@B_{12}H_{12}^{2-}$ cluster, which dissociates into He and $B_{12}H_{12}^{2-}$ with a moderate exothermicity, the usual saddle point optimization procedures with only initial force constant calculations [i.e., opt = (ts,calcfc)] as well as the quadratic synchronous transit (opt = qst2) procedures proved to be inefficient. Neither approach converged after more than 100 optimization cycles due to oscillations of the He atom inside the cage. The most successful procedure was the time-demanding optimization with recalculation of force constants at each step [opt = (ts,calcall)]. Although all these searches were carried out without any symmetry constraints, the optimized transition structure has C_2 symmetry (**TS-1** in Figure 3). The single imaginary frequency eigenvector is directed along the 2-fold molecular axis toward the "active" B−B edge 4−6. The cage in **TS-1** is deformed and its geometry differs substantially from the initial icosahedron symmetry. The "active" edge 4−6 is stretched to over 3.3 Å, and the attached hydrogen atoms H_{16} and H_{18} are twisted strongly in opposite directions. In the transition state the He atom, located on a 2-fold axis, has moved only ∼0.6 Å from its location in the former center of the icosahedron. NBO population analysis indicates that this He shift is accompanied by significant redistribution of electron density from atoms B_4 and B_6 of the "active" edge (by 0.45 *e* from each of them) to the neighbor cage atoms, mostly B_1, B_5, B_7, and B_{10}. Intrinsic reaction coordinate (IRC) calculations at B3LYP/6-31G* confirmed that **TS-1** lies on the minimal energy pathway for expulsion of He from the cage and connects the endohedral structure **1** with the decomposition products He + $B_{12}H_{12}^{2-}$.

The barrier height in $He@B_{12}H_{12}^{2-}$ relative to structure **1** is calculated to be 63.5 kcal/mol at B3LYP/6-31G* with ZPE correction. This result confirms our earlier conclusion[12] concerning the high kinetic stability of icosahedral clusters with an internal He atom. However, the energy of structure **2** (C_2), where He was fixed in the center of the broken 4−6 edge, is

(22) Schleyer, P. v. R.; Maerker, C.; Dransfeld, A.; Jiao, H. J.; Hommes, N. *J. Am. Chem. Soc.* **1996**, *118*, 6317.

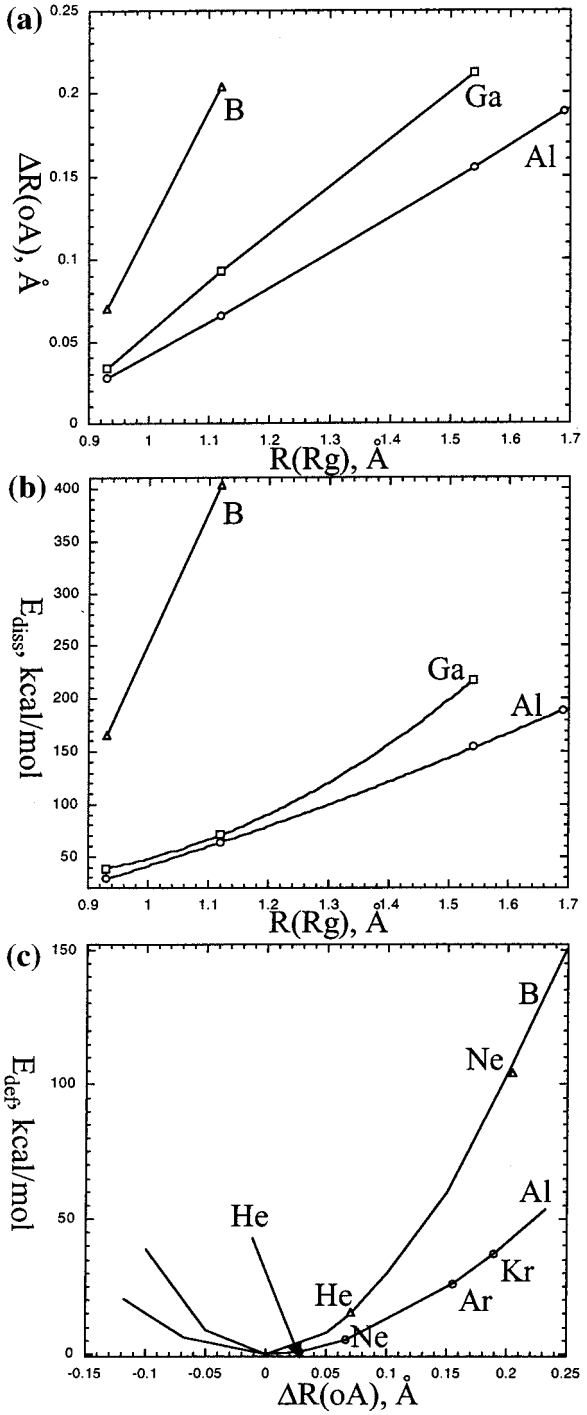

Figure 2. Dependence of endohedral $Ng@A_{12}H_{12}^{2-}$ cluster structure and energy parameters on the Ng atomic radius (R(Ng)): (a) ΔR(oA)/R(Ng), Å; (b) E_{diss}/R(Ng), kcal/mol; (c) $E_{def}/\Delta R$(oA), kcal/mol. R(oA) is the distance between the center and a vertex of the $A_{12}H_{12}^{2-}$ icosahedron, E_{diss} is the exothermicity of the $Ng@A_{12}H_{12}^{2-} \rightarrow Ng + A_{12}H_{12}^{2-}$ reaction, and E_{def} is the cage strain energy due to Ng insertion. The last was based on the energy difference between the relaxed and deformed cage (without the Ng atom).

~38 kcal/mol less than **TS-1**. Hence, although **2** can easily be calculated by partial optimization, its relative energy provides only a crude estimate of $H_{exit}^{\ddagger}$ in boranes.

The $Ne@B_{12}H_{12}^{2-}$ cluster is extremely strained, and the endohedral atom expulsion reaction is highly exothermic. However, we were able to locate the TS easily using the quadratic synchronous transit method (also without symmetry constraints). The calculated TS structure (**TS-2** in Figure 3) essentially converged to C_{3v} symmetry. The Ne atom is located on the 3-fold axis and shifted from the icosahedron center toward a face by only ~0.10 Å. However, the B−B edges in the "breaking" face have elongated from 1.86 Å (structure **1**) to ~2.4 Å in **TS-2**. IRC calculations showed that when the Ne atom moves from its position in **TS-2** toward the cage face by 0.1 Å along the minimal energy reaction path, the B−B edges of this face lengthen by an additional 0.25 Å. In the optimized C_{3v} model structure **3**, where Ne was fixed in the center of the broken face, the distances between atoms 1−2−3 are longer, ~3.3 Å, but the energy of **TS-2** is about 90 kcal/mol higher than **3**. The barrier height $H_{exit}^{\ddagger}$ calculated relative to structure **1** is only 2.6 kcal/mol with the ZPE correction. Thus, the $Ne@B_{12}H_{12}^{2-}$ cluster stability is predicted to be very low.

The character of the potential energy surface (PES) and that of the expulsion TS's change drastically for the less rigid alane clusters. The initial geometry in the $He@Al_{12}H_{12}^{2-}$ TS search was based on **2**, similar to **TS-1** for $He@B_{12}H_{12}^{2-}$. The structure changed dramatically, and the optimized (also without symmetry restrictions) TS acquired an unusual open shape with large deformations in the "active" hemisphere of the cluster (see **TS-3** in Figure 3). **TS-3** possesses C_s symmetry and resembles a "pot with open lid" where the "capping" Al_6–H_{18} group is strongly shifted away from the 5-fold C_5 axis, and among five former bonds of Al_6 with neighbor cage atoms, only two, Al_6–Al_1 and Al_6–Al_5, remain, while the other edges including the base of the "lid" Al_1–Al_5 are broken. In contrast to **TS-1** (for $He@B_{12}H_{12}^{2-}$) and **TS-2** (for $Ne@B_{12}H_{12}^{2-}$) where the heteroatoms are still located inside the cages, the He atom has nearly exited the cage in **TS-3** (for $He@Al_{12}H_{12}^{2-}$). The most favorable exit pathway through a pentagonal aperture with a larger number of broken and elongated Al−Al bonds[23] can be described as a "decapping" mechanism. $H_{exit}^{\ddagger}$ for $He@Al_{12}H_{12}^{2-}$ (58.5 kcal/mol including ZPE), only ~8 kcal/mol lower than $H_{exit}^{\ddagger}$ for $He@B_{12}H_{12}^{2-}$, is large enough to ensure a large kinetic stability of the $He@Al_{12}H_{12}^{2-}$ cluster predicted earlier.[12]

The $Ne@Al_{12}H_{12}^{2-}$ TS search (at B3LYP/6-31G*) used three different initial geometries corresponding to **TS-1**, **TS-2**, and **TS-3**, but only the opened **TS-3a** resulted (Figure 3). In contrast to $He@Al_{12}H_{12}^{2-}$ **TS-3**, in **TS-3a** the Ne atom remains closer to the icosahedron center despite the significant deformations of Al−Al bonds seen throughout the skeleton. The barrier $H_{exit}^{\ddagger}$ for Ne exit from $Ne@Al_{12}H_{12}^{2-}$ via **TS-3a** is 44.4 kcal/mol relative to structure **1**. This barrier is ~17 kcal/mol lower than that for $He@Al_{12}H_{12}^{2-}$, but still high enough to guarantee the kinetic stability of $Ne@Al_{12}H_{12}^{2-}$.

Like the He and Ne analogues, the exit transition state for $Ar@Al_{12}H_{12}^{2-}$ has a **TS-3** type structure (see **TS-3b** in Figure 3). In this TS, Ar is located even closer to the center of the icosahedron than Ne in **TS-3a**, and the cage deformations are severe. $H_{exit}^{\ddagger}$ is 15.2 kcal/mol and $Ar@Al_{12}H_{12}^{2-}$ is kinetically much less stable than its lighter analogues. Its existence apparently would be possible only in low-temperature inert matrixes, in combination with bulky cations. Because the cage strain is so high in $Ar@Al_{12}H_{12}^{2-}$ (as in $Ne@B_{12}H_{12}^{2-}$), even small 0.3 Å displacements of Ar from the cage center in **TS-3b** result in very strong deformation of the skeleton and rupture of a number of Al−Al bonds. The structure of the

(23) Assignment of the number of "ruptured" A−A bonds in the TS of elastic clusters like $Ng@Al_{12}H_{12}^{2-}$ often is not simple since the entire cage is strained and various edges are elongated considerably. Therefore, the boundary between "completely ruptured" and "strongly stretched" bonds is not clear.

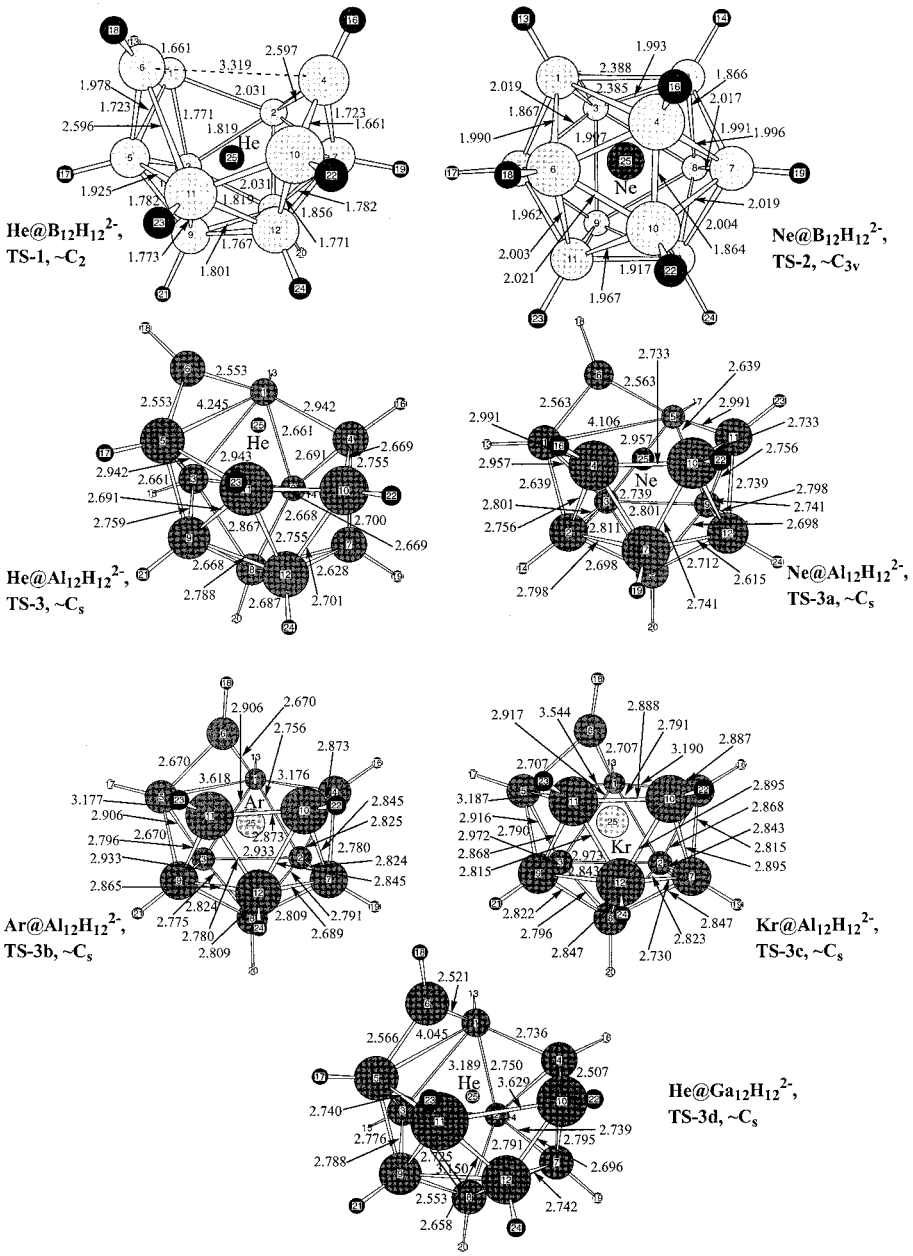

Figure 3. B3LYP/6-31G* optimized transition structures for the $Ng@A_{12}H_{12}^{2-} \rightarrow Ng + A_{12}H_{12}^{2-}$ reaction. The B3LYP/SDD method was employed for $He@Ga_{12}H_{12}^{2-}$, **TS-3d**. In **TS-3**, $He@Al_{12}H_{12}^{2-}$, the He atom is roughly located in the middle of a planar pentagon with average R(He−Al) ≈ 2.6 Å and displacement above the plane of ∼0.1 Å.

transition state **TS-3c** for $Kr@Al_{12}H_{12}^{2-}$ is quite similar to that of **TS-3b**, with the barrier $H_{exit}^{\ddagger}$ of 10.5 kcal/mol, so this species is expected to be the least stable kinetically among the alane clusters.

The alanes with He, Ne, Ar, and Kr show a clear trend, based on simple steric considerations, which characterize the **TS-3** type transition states: with increasing noble gas atom radius the barrier height $H_{exit}^{\ddagger}$ drops rapidly, the torsion angle between the planes of triangular "lid" and pentagonal aperture and the Ng atom shift from the icosahedron center toward the attacked vertex in TS also decrease (in this sense, TS geometry develops sooner), and the rupture and elongation of the Al−Al bond is less localized to the active hemisphere and involves the entire cage. Similar trends can be expected for the gallanes and related electron-deficient clusters with dense, elastic cages (e.g., indanes, $X@In_{12}H_{12}^{2-}$, thallanes, $X@Tl_{12}H_{12}^{2-}$, and "naked" aluminides, $X@Al_{12}^{4-}$). The largest changes may be anticipated in going from Ne to Ar because the largest change in the size of Ng occurs (N.B. the effect of Ne/Ar interchange in structure **1**, above).

Our gallane studies were less extensive. B3LYP/SDD transition state optimization of $He@Ga_{12}H_{12}^{2-}$ used the Stuttgart−Dresden effective core potential for Ga atoms.[24] The He exit transition state similar to **TS-3** resulted in **TS-3d** (see Figure 3). The He atom lies below the plane of the uncovered pentagonal aperture, and deformations of all the cage bonds are large. The **TS-3d** barrier height is about 32 kcal/mol. However, the effective core potential approach is less reliable than the all-electron B3LYP/6-31G* method. Note that our parallel B3LYP/6-31G* and B3LYP/SDD calculations on He and Ne

(24) (a) Dolg, M.; Wedig, U.; Stoll, H.; Preuss, H. *J. Chem. Phys.* **1987**, *86*, 866. (b) Dolg, M.; Stoll, H.; Preuss, H. *J. Chem. Phys.* **1989**, *90*, 1730. (c) Kaupp, M.; Schleyer, P. v. R.; Stoll, H.; Preuss, H. *J. Chem. Phys.* **1991**, *94*, 1360.

alanes and gallanes show systematic differences between the two methods. The Ga−Ga bond lengths in the B3LYP/SDD optimized icosahedral structure are 0.20−0.25 Å larger than at B3LYP/6-31G*, vibrational frequencies are underestimated, and the alane transition states, although of the **TS-3** type, are strongly deformed and lose C_s symmetry. Therefore, we can only conclude qualitatively that gallane endohedral clusters should be less stable kinetically than the corresponding alane clusters.

Since the transition states for all alanes and gallanes considered here belong to the **TS-3** type, one can expect that the "decapping" mechanism for expulsion of the endohedral atom will be a feature of other related electron-deficient clusters formed by the third row atoms and heavier elements. In contrast, clusters of light second row elements, with strong σ- and π-bonds, should find this pathway significantly less favorable as compared, for instance, with an exit via the cage edge.

Influence of External Cations. Because of the close relationship to the $Ng@A_{12}H_{12}^{2-}$ dianions, we performed similar calculations on $Li[Ng@A_{12}H_{12}]^-$ anions and neutral $Li_2[Ng@A_{12}H_{12}]$ molecules. The influence of external cations on cluster structure and stability was assessed with the structures **4**, C_{3v} (one Li^+ cation located above a cage face) and **5**, D_{3d} (two Li^+ cations located above opposite cage faces) (Figure 1). These structures are local minima. The related empty anion systems $L[A_{12}H_{12}]^-$, with H^+, Al^+, Al^{3+}, alkali metal, and alkaline earth metal cations coordinated, were investigated carefully earlier.[12] We compare the results for empty and Ng-centered salts here and concentrate on the peculiarities caused by the presence of the internal atom Ng.

As expected, the cation influences differ substantially and correlate with the exothermicities of the $Ng@A_{12}H_{12}^{2-} \rightarrow Ng + A_{12}H_{12}^{2-}$ reactions. In $He@Al_{12}H_{12}^{2-}$ or $He@Ga_{12}H_{12}^{2-}$, where skeletal strain is small, the presence of He does not change the deformation of the $A_{12}H_{12}^{2-}$ anion in the field of a cation significantly. The coordinated face in **4** expands, the opposite face contracts, the bridging H_b hydrogen atoms are shifted toward the Li^+ cation, and there is a parallel decrease in the H_bALi angle and the elongation in the $R(A-H_b)$ distance. Deformations of the less rigid alanes are much larger than the boranes, especially when the cation radii are small and the cations are multiply charged. Degenerate vibrational frequencies and orbital energies split when the cation field reduces the symmetry from I_h to C_{3v} or D_{3d}. The exothermicity of He expulsion from the alane and the borane cages increases for $Li[He@A_{12}H_{12}]^-$ compared with $He@A_{12}H_{12}^{2-}$ by just a few kilocalories per mole. The increase in exothermicity for boranes is 10 kcal/mol, but this change does not exceed 6% E_{diss}.

The cation−anion interaction can drastically change the structure of systems with very exothermic E_{diss} and with a large Ng atom inside. The cage strain is large and the influence of the cation may even be sufficient to overcome the dissociation threshold and lead to expulsion of Ng from the cage. For example, Li^+ coordination to $Ne@B_{12}H_{12}^{2-}$ causes the Ne atom to exit from the cage without barrier: structure **4** dissociates into Ne and $LiB_{12}H_{12}^-$. However, **4** corresponds to a local minima for $Ne@Al_{12}H_{12}^{2-}$ and for $Ne@Ga_{12}H_{12}^{2-}$. The aluminum and gallium cages in **4** are deformed by the Li^+ cations to approximately the same extent as in the C_{3v} $LiAl_{12}H_{12}^-$ and $LiGa_{12}H_{12}^-$ anions. In other words, the metastable $Ne@B_{12}H_{12}^{2-}$ becomes unstable even when it is disturbed by one Li^+ cation. Our calculations on the $Na[Ne@B_{12}H_{12}]^-$ and $Al[Ne@B_{12}H_{12}]^-$ systems showed that replacement of Li^+ with the larger Na^+ and Al^+ cations does not change the result; in both cases Ne leaves the cage without a barrier.

The combined effects of two Li^+ cations coordinated to opposite faces of the $Ng@A_{12}H_{12}^{2-}$ icosahedrons in boranes strongly differ from those in alanes and gallanes due to the differences in the strengths of the A−A bonds. For instance, the closo structure **5** is maintained in $Li_2[He@B_{12}H_{12}]$ where the borane cage is only slightly deformed as compared to the $He@B_{12}H_{12}^{2-}$ anion. The B−B bond lengths in this salt are in the 1.822−1.879 Å range, close to 1.861 Å in $He@B_{12}H_{12}^{2-}$, and the B−H bond lengths change within 0.01−0.02 Å. The geometry deformation from the empty $Li_2B_{12}H_{12}$ salt to endohedral $Li_2[He@B_{12}H_{12}]$ is rather similar to that discussed for the anions $B_{12}H_{12}^{2-}$ and $He@B_{12}H_{12}^{2-}$. In contrast, the closo structures of the less rigid alane $Li_2[He@Al_{12}H_{12}]$ and gallane $Li_2[He@Ga_{12}H_{12}]$ salts are destroyed: the equatorial two-center Al−H bonds transform into three-center bridging bonds, and the D_{3d} structures **5** optimize in D_{3d} symmetry without barriers into new, unusual structures **6** where only some of the of Al−Al and Ga−Ga bonds remain. Structure **6** for both the alane and the gallane have one a_{1u} imaginary frequency which corresponds to the transition state for complex intramolecular rearrangements. Apparently, even the kinetically stable Ng alane and gallane dianions would be stable in salts only with bulky countercations.

Conclusions

We have computed related *closo*-boranes, -alanes, and -gallanes $Ng@A_{12}H_{12}^{2-}$ with noble gas atoms inside the $[A_{12}]$ cages. The icosahedral endohedral structures **1** are local minima, significantly higher in energy than the $Ng + A_{12}H_{12}^{2-}$ dissociation limits for $He@B_{12}H_{12}^{2-}$, $Ne@B_{12}H_{12}^{2-}$, $He@Al_{12}H_{12}^{2-}$, $Ne@Al_{12}H_{12}^{2-}$, $Ar@Al_{12}H_{12}^{2-}$, $Kr@Al_{12}H_{12}^{2-}$, $He@Ga_{12}H_{12}^{2-}$, and $Ne@Ga_{12}H_{12}^{2-}$. The exothermicity of the expulsion of Ng from a cage increases rapidly with increased noble gas atomic radius. E_{diss} is very large for boranes (166 and 403 kcal/mol with Ng = He and Ne, respectively) and much smaller for alanes (29, 63, 154, and 189 kcal/mol for Ng = He, Ne, Ar, and Kr, respectively), but the values for the gallanes (39 and 71 kcal/mol with Ng = He and Ne, respectively) are somewhat larger than those for the alanes.

There are three types of Ng exit transition state: via an edge (**TS-1**); through a face (**TS-2**); and via a pentagonal "neck" of the cage, much like a "pot with open lid" (**TS-3**). These favored TS types in different clusters depend on the cage rigidity, the expulsion reaction exothermicity, and the relation between the size of cage internal cavity and the internal Ng atomic radius. When dissociation is only moderately exothermic (e.g., alanes and gallanes with He and Ne inside), Ng exit via a pentagonal "neck" is preferred (**TS-3**). In $He@B_{12}H_{12}^{2-}$ exit occurs via a cage edge (**TS-1**). In $Ne@B_{12}H_{12}^{2-}$, which has the largest dissociation exothermicity, the exit occurs via a triangular face (**TS-2**). $H_{exit}^{\ddagger}$ is quite high (30−60 kcal/mol) for all helium-containing clusters, but the barriers are lower for the $Ne@Al_{12}H_{12}^{2-}$ and $Ne@Ga_{12}H_{12}^{2-}$ systems (e.g., $Ar@Al_{12}H_{12}^{2-}$ and $Kr@Al_{12}H_{12}^{2-}$ barriers are about 15 and 10 kcal/mol, respectively) and the kinetic stability of these systems is low. The $Ne@B_{12}H_{12}^{2-}$ cluster has a very low barrier and is not expected to be observable.

The $Ng@A_{12}H_{12}^{2-}$ cage geometry exhibits a linear dependence on the atomic radius of the internal noble gas. NMR chemical shifts for He atoms in the clusters are negative, while for the other Ng's NMR chemical shifts are positive and have much larger values. NICS values indicate that all three $A_{12}H_{12}^{2-}$ anions are highly aromatic with the alanes somewhat less so. Charge transfer between the internal atom and cage is insig-

nificant in clusters with He and Ne, so that steric and electronic repulsion between the closed electronic shells of Ng and $A_{12}H_{12}^{2-}$ play a crucial role in the heteroatom−cage interactions. A medium intense t_{1u} band in the 925−1030 cm^{-1} region for boranes and 340−560 cm^{-1} for alanes and gallanes corresponding mainly to vibrations of the internal atom should be the most characteristic feature of IR spectra of $Ng@A_{12}H_{12}^{2-}$ systems.

The effect of one external Li^+ located above a cage face of the lithium salts $Li[Ng@A_{12}H_{12}]^-$ is not large in the helium clusters. However, in systems such as $Li[Ne@B_{12}H_{12}]^-$, which have extremely large expulsion exothermicities, the internal atom exits from the cage and the salt dissociates into $Ne + LiB_{12}H_{12}^-$ without a barrier. Systems with two Li^+ ions located above opposite cage faces, ($Li_2[Ng@A_{12}H_{12}]$), undergo complex intramolecular rearrangements which destroy the skeletal closo structure.

Acknowledgment. This work was supported by Academia Sinica and the National Science Council of Republic Of China under Grants NSC 8902113-M-001-069 and 90-2113-M-001-068. O.P.C. and N.M.K. thank the National Science Council of Republic Of China and Academia Sinica for their visiting fellowships at IAMS and also the University of Georgia for providing financial support for their visit to the Center for Computational Quantum Chemistry.

Supporting Information Available: Optimized Cartesian coordinates of various local minima and transition states. This material is available free of charge via the Internet at http://pub.acs.org.

IC010573S